Last author copy - Paper presented at the 7th IAASS Conference in Friedrichshafen (Germany), 20-22 October 2014

SMALL DEBRIS FRAGMENTS CONTRIBUTION TO COLLISION PROBABILITY FOR SPACECRAFT IN LOW EARTH ORBITS

Francesca Letizia[(1)], Camilla Colombo[(2)], Hugh G. Lewis[(3)]

[(1)]*Astronautics Research Group, University of Southampton, Southampton, SO17 1BJ United Kingdom, Email: f.letizia@soton.ac.uk*

[(2)] *Department of Aerospace Science and Technology, Politecnico di Milano, 20156 Milan, Italy, Email: camilla.colombo@polimi.it*

[(3)]*Astronautics Research Group, University of Southampton, Southampton, SO17 1BJ, United Kingdom, Email: H.G.Lewis@soton.ac.uk*

ABSTRACT

Around the Earth there are more than ten million objects larger than 1 mm that can interfere with other orbiting spacecraft. In particular, objects larger than 1 cm are considered massive enough to seriously damage or even destroy a satellite in case of collision. The traditional piece-by-piece approach to study the evolution of debris objects cannot be applied to small fragments their number is so large that the computational time would be prohibitive. This work proposes an alternative method based on the computation of the fragment density, whose evolution in time under the effect of atmospheric drag can be obtained with the continuity equation. The fragment density can then be used to evaluate the resulting collision probability. In particular, the proposed method is here applied to evaluate the consequence of some reference breakups on a list of target objects. In addition, the low computational time allows simulating many collision scenarios with different collision conditions to understand which parameters have the largest effect on the risk for other spacecraft.

1. INTRODUCTION

Around the Earth there are more than 500 000 objects larger than 1 cm and more than ten millions objects larger than 1 mm. Objects of this size are considered to be able to interfere with operational spacecraft either causing anomalies in their operations and, for larger fragments, causing the loss of the satellites [1]. In fact, fragments larger than 1 cm cannot even be stopped by the shields currently adopted on the International Space Station (ISS). Moreover, objects smaller than 10 cm cannot be tracked with current radar technology. As a result, small fragments contribution to the collision probability is often neglected (excluding the studies in [2, 3]).

In addition, even if new radars technologies will enable to detect and track smaller fragments, the size of the database of possible colliding particles will remarkably increase and the computational time will become prohibitive if each fragment is individually followed. Some of the existing methods tackle this problem by defining some representative objects that group a set of small fragments. The representative objects are then propagated and the original picture of the small fragments is then reconstructed *a posteriori* [4].

This work proposes instead a different and novel approach based on the definition of the density of fragments. The total object density is propagated instead of following each single fragments. The density is then used directly to compute the resulting collision probability. Besides this advantage, this formulation of the problem allows adopting an analytical method for the propagation. In fact, if only the effect of atmospheric drag is considered, the cloud density evolution can be obtained by applying the continuity equation as originally proposed by McInnes [5].

The continuum approach was used in different fields of astrodynamics, including applications to model the evolution of global space debris evolution [5], interplanetary dust [6, 7] and swarm satellites [8]. Here it is used to model the debris cloud resulting from a collision in Low Earth Orbit (LEO) and evaluate its impact on the collision probability for other spacecraft.

The paper is structured as follow: Section 2 gives a brief overview on the method used to propagate debris clouds with the continuity equation and Section 3 on the hypotheses and method to compute the resulting collision probability. Section 4 presents some possible applications of the method, such as, for example, the assessment of the collision risk caused by a small breakup and the identification of the most critical conditions of collision for a set of spacecraft.

2. DEBRIS CLOUD PROPAGATION

When two objects collide in space, a cloud of fragments is generated: the cloud is initially dense (Fig. 1a), but with time it spreads around the Earth, forming a band whose extension in latitude is limited by the inclination of the orbit where the collision occurred (Fig. 1c).

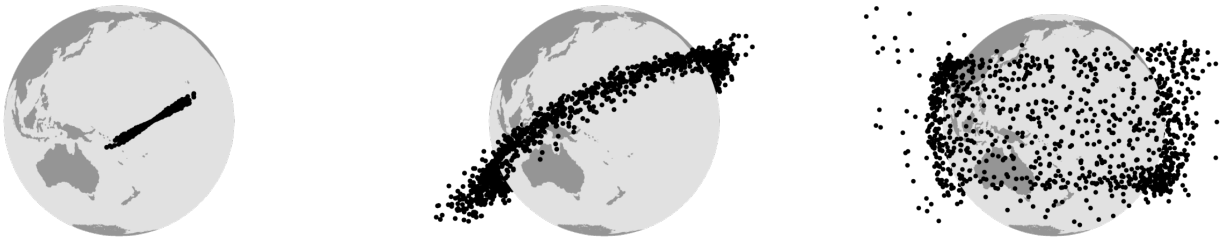

(a) Ellipsoid *(b) Toroid* *(c) Band*

Figure 1: Phases of debris cloud evolution as classified by McKnight [9] and Jehn [10]. The simulation refers to a collision on a parent orbit with inclination equal to 30°

McKnight [9] proposed a phased approach to study the cloud evolution where its transition from one state to the other in Fig. 1 can be explained with the effect of a dominating force. The method employed in this work uses different techniques to model each phase in order to obtain the long term evolution of the fragment cloud. The details of the method can be found in [11] and here they are only summarized.

A collision produces a cloud of fragments, whose number depends on the energy of the event. Breakup models available in literature can be used to estimate the features of the fragments (e.g., their mass) and how the energy is distributed among the fragments. In particular, the NASA breakup model [12, 13] is here used, considering fragments with size between 1 mm and 8 cm. In the initial phase, the cloud is compact and localized at the collision location; then, as each fragment has a different energy, the cloud is gradually spread along the whole orbit.

On longer time scale, in the order of months, the effect of perturbations becomes relevant. In particular, the Earth's oblateness rotates each fragment orbit spreading the cloud to form a band around the Earth. In our method, this phase is modeled with the numerical propagation of the fragments orbital parameters under the effect of the Earth's oblateness (considering only the J_2 term) and drag (adopting an exponential model for the atmospheric density). The average expression of the orbital dynamics is used [14]. The numerical propagation is stopped once the band is formed, using Ashenberg's [15] theory to estimate the time necessary for this process.

Once the band is formed, it is possible to switch the point of view from the study of the single fragments to the evaluation of the cloud spatial density. It is important to highlight that this can be done only at this stage as the formation of the band means that the argument of the perigee (ω) and the longitude of the ascending node (Ω) are randomized. In other words, at the band stage there is a radial symmetry, so the problem can be studied considering only the dependence on the distance r. As the band is limited in latitude, the problem should consider also the dependence on the latitude, which depends on the inclination of the orbit where the fragmentation took place. Actually, as it will be explained in detail in Section 3.1, the distribution in latitude and the one in distance can be studied separately. Here the focus is on the distribution as a function of distance that is directly affected by the atmospheric drag and therefore drives the long term evolution of the cloud.

The distribution in r is built starting from the knowledge of the fragment orbital parameters and applying Kessler's expression [16]

$$n(r,t_0) = n_0(r) = \frac{1}{4\pi r a} \frac{1}{\sqrt{e^2 - \left(\frac{r}{a} - 1\right)^2}}. \qquad (1)$$

This expression is preferred here instead of the one used in the previous version of the method [11] because it is more effective in describing the fragment distribution. This is especially true for the representation of the peak height, which has a relevant impact on the computation of the collision probability. This new version of the method was evaluated with the same criteria in [11] and it proved to have the same applicability range in terms of altitude, namely from 800 km and above [17].

Once the fragment spatial density at the band formation (n_0) is defined, its evolution in the long term is immediately known thanks to the continuity equation. It is written as

$$\frac{\partial n(r,t)}{\partial t} + \nabla \bullet \mathbf{f}(\mathbf{r},\mathbf{t}) = \dot{n}^+ - \dot{n}^-, \qquad (2)$$

were $\nabla \bullet \mathbf{f}$ accounts for the *slow*/continuous phenomena (e.g., the effect of perturbations) and $\dot{n}^+ - \dot{n}^-$ the *fast*/discontinuous events (e.g., the injection of new fragments due to launches). Fast events are not considered here ($\dot{n}^+ - \dot{n}^- = 0$), whereas the term $\nabla \bullet \mathbf{f}$ is used to model the effect of drag.

The method of characteristics allows transforming Eq. 2 into a system of Ordinary Differential Equations (ODE) that admits an explicit solution for the evolution of the fragment density, under the approximations of an exponential model for the atmosphere and of quasi-circular orbits for the fragments [5]. With the exponential model,

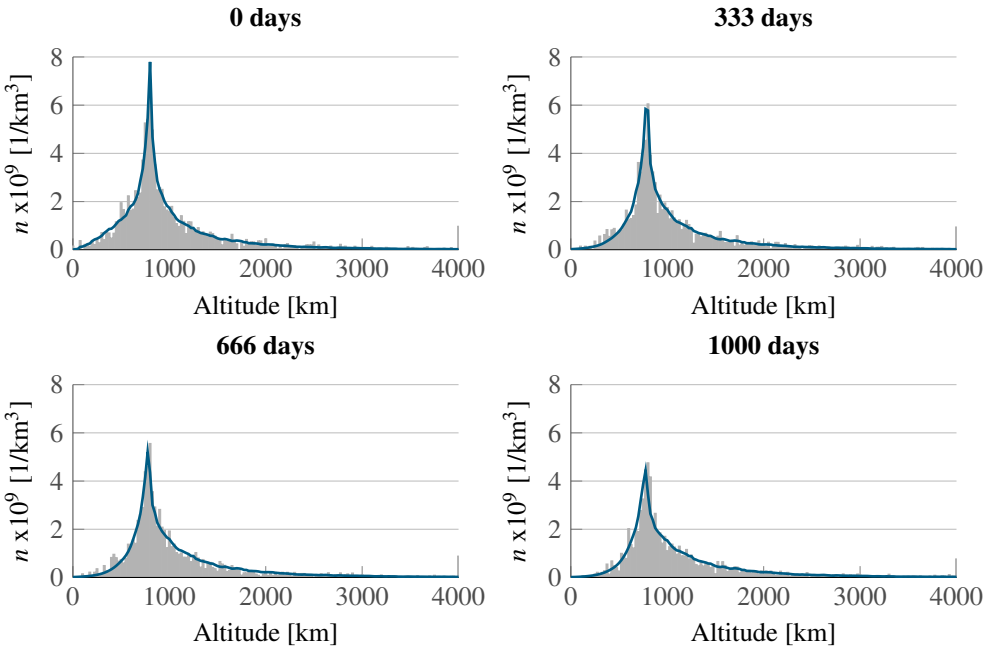

Figure 2: Fragment spatial density for a fragmentation at 800 km, on a planar orbit. The band is formed after 95 days and the time on top of each plot is measured from that moment. The gray bars represent the distribution of fragments obtained with the numerical propagation, the blue line represents the result of the analytical propagation

the expression of the atmospheric density at altitude r is

$$\rho = \rho_H \exp\left(\frac{r-R_H}{H}\right)$$

where ρ_H and H are, respectively, the density and scale height at the reference altitude R_H. With this expression of the atmospheric density, the spatial density can be written as a function of of distance r and time t

$$n(r,t) = \frac{\Psi\{\exp[-\frac{r-R_H}{H}] + (\varepsilon\sqrt{R_H}/H)t\}}{-\varepsilon r^{5/2}\exp[-\frac{r-R_H}{H}]}, \qquad (3)$$

where Ψ is a function obtained from the initial condition $n_0(r)$ [11] and ε is a parameter of the problem that collects all the terms not depending on r

$$\varepsilon = \sqrt{\mu}\frac{c_D A}{M}\rho_H. \qquad (4)$$

In Eq. 4, μ is the gravitational constant of the Earth and c_D, A, M are the ballistic coefficient, the cross area and the mass of the fragments. The same value of c_D is used for all fragments and is set equal to 2.2 [18]. The area-to-mass ratio A/M has instead a large variation among the fragments [12], so the cloud is divided into $N_B = 10$ bins in A/M and the total cloud density is obtained by summing the partial densities in each A/M bin

$$\begin{aligned} n(r,t) &= \sum_i^{N_B} n_i(r,t) \\ &= \sum_i^{N_B} \frac{\Psi\{\exp[-\frac{r-R_H}{H}] + (\varepsilon_i\sqrt{R_H}/H)t\}}{-\varepsilon_i r^{5/2}\exp[-\frac{r-R_H}{H}]} \end{aligned} \qquad (5)$$

whose evolution is obtained defining an average value of ε_i for each A/M bin.

Fig. 2 shows an example of the evolution of the cloud density with time obtained with the explained method. The fragmentation studied in Fig. 2 occurred at 800 km, on a planar orbit; the band is formed after 95 days and from that moment the analytical propagation is used. The distribution of fragments in altitude obtained with the numerical propagation is plotted with the the gray bars, while the blue line represents the result of the analytical propagation, which shows a good agreement with the numerical data. The advantage of the analytical method is that this result, which represent the propagation of a cloud of 2397 fragments for 1500 days after the fragmentation, is obtained with a computational time of less than 13 s on a PC with 8 CPUs at 3.40 GHz; as a reference, the computational time required to propagate numerically each fragment is instead more than 130 s.

3. COLLISION PROBABILITY

Following Kessler's [16] approach, the collision probability for a target crossing the cloud is computed considering the average number of collisions at a given time t. This can be written as

$$N = F\sigma t \qquad (6)$$

where F is the flux of particles

$$F = SV \qquad (7)$$

with V the average relative velocity and S the fragment density function of the distance and the latitude β

$$S(r,\beta) = s(r)f(\beta)$$

In Eq. 6 σ represents the collisional cross-sectional area. This is usually defined considering the dimensions of both the colliding objects [16], but here only the target spacecraft area is considered because the fragments are much smaller than it.

For the spatial density $s(r)$, the value of density $n(r,t)$ obtained with the method explained in Section 2 is used. This approach was validated by verifying that the error compared to the distribution obtained from the numerical propagation is acceptable also for long simulations. In particular, the method is able to simulate the cloud evolution for five years with a relative error lower than 20% for altitudes equal and larger than 800 km [17].

As said the proposed approach can be used only to model the impact of the cloud after the band is formed, therefore future work will aim to estimate the collision probability also in the first phases of the cloud evolution. Here, instead, the focus is on the long term contamination of space environment.

In order to keep the model simple and dependent on the distance only, the average relative velocity between the fragments and the target V is computed with the expressions in [16] assuming that the average collision angle is 90° and that the fragments and the target are on similar quasi-circular orbits. Therefore, V is set equal to $\sqrt{2}$ times the orbital speed for a circular orbit at the target altitude r_T

$$V \approx \sqrt{2} v_{\text{orb}} = \sqrt{\frac{\mu}{r_T}}. \tag{8}$$

This approximation was evaluated by simulating different collision scenarios, changing both the target and the fragmentation parameters. In all the tested cases, Eq. 8 overestimates the valued of the average relative velocity with a maximum relative difference of 10% [17].

Finally, the cumulative collision probability is obtained with the expression

$$P_c = 1 - \exp(\sigma n(r,t) V \Delta t), \tag{9}$$

following the common analogy with the kinetic gas theory [19, 9]. The time frame for the computation is five years and the used Δt is equal to 3.5 days for the results shown in Section 4.

3.1. The role of latitude

The expression in Eq. 1 expresses the fragment density computed in a spherical volume around the Earth. However, as shown in Fig. 1, the fragments are distributed in a band limited in latitude by the inclination of the parent orbit i_0. For retrograde orbits, the latitude is obviously limited by $\pi - i_0$, but for simplicity the following equations are given considering i_0 defined between 0 and $\pi/2$.

To describe the dependence on the latitude β, Kessler [16] multiplies the spatial density $n(r)$ by a function $f(\beta)$ that represents the distribution in latitude

$$f(\beta) = \begin{cases} 0, & \text{if } |\beta| > i_0 \\ \frac{2}{\pi} \frac{1}{\sqrt{\sin^2 i_0 - \sin^2 \beta}}, & \text{if } |\beta| \leq i_0. \end{cases} \tag{10}$$

Differently from the spatial density n, the distribution in β is not affected directly by the atmospheric drag. This means that the dependence on the latitude could be easily included also in the method proposed in this work, multiplying the expression by the spatial density $n(r,t)$ in Eq. 3 by the function $f(\beta)$ in Eq. 10. However, the target latitude β is a fast variable, compared to the evolution of the orbital parameters. Therefore, in this work, an average value is used

$$\bar{f}(\beta) = \begin{cases} 0, & \text{if } |\beta| > i_0 \\ \frac{1}{\sin i_0}, & \text{if } |\beta| \leq i_0. \end{cases} \tag{11}$$

By using this approach, the spatial density is correctly rescaled to consider the actual volume occupied by the fragments. Moreover, it also allows integrating the target trajectory more quickly, without using a small integration step to follow the evolution of the latitude.

4. COLLISION SCENARIOS

The method explained in Sections 2 and 3 can be applied to study the collision probability due to small fragments in different scenarios as the computational time is much lower than the one of numerical propagation. Here, two possible applications are presented: firstly, the impact of a breakup on different target spacecraft is evaluated; secondly, for each target spacecraft a *map* of collision probability is built by varying the inclination and the altitude of the simulated breakup.

In both case, a list of *interesting* targets is required. Here we used the one prepared by IFAC-CNR, ISTI-CNR and University of Southampton for a study sponsored by the European Space Agency [20]. The list was sorted by the computed cumulative collision probability and only spacecraft are considered (i.e., no rocket bodies or objects released in operation are analyzed). Tab. 1 summarized the relevant information for the first ten spacecraft in the list; in detail, Tab. 1 indicates the spacecraft ID used in this work and the one in MASTER population; it also reports the altitude of the perigee h_p, the altitude of the apogee h_a, the spacecraft inclination i, the mass and the size of the spacecraft, the cumulative collision probability P_c.

Table 1: List of target spacecraft [20] for the collision probability analysis

ID	Target	h_p [km]	h_a [km]	i [deg]	Mass [kg]	Size [m]	P_c
1	ESA-3926	842.6304	855.6396	70.98	3200	6.33	1.77E-01
2	ESA-4419	816.0959	818.9741	98.73	4090	6.91	1.75E-01
3	ESA-3692	842.9113	863.1587	71.00	3200	6.33	1.70E-01
4	ESA-3541	762.9208	764.3492	98.45	8110	8.96	1.66E-01
5	ESA-271	799.7443	806.9258	64.90	16800	7.11	1.66E-01
6	ESA-3410	837.8654	855.2046	70.99	3200	6.33	1.64E-01
7	ESA-3847	815.9959	818.8741	98.67	4090	6.91	1.63E-01
8	ESA-3047	830.2175	863.4525	70.90	3220	6.23	1.60E-01
9	ESA-3189	820.5950	823.4750	98.54	2730	5.74	1.43E-01
10	ESA-253	790.9662	796.7038	85.00	4580	5.78	1.33E-01

4.1. Single event impact

The first application of the method is the evaluation of the consequences of a breakup on the target list in Tab. 1, also considering the different collision probability associated with fragments larger than 1 cm or larger than 1 mm.

For this application, two recent small breakups are considered [21], whose parameters are reported in Tab. 2. The value in the last column is a measure of the energy of the breakup. It is the parameter that in the NASA breakup model [12] is used to define the fragment size distribution for a collision through the expression

$$N(L_c) = 0.1(M_E)^{0.75} L_c^{-1.71} \tag{12}$$

where L_c is the fragment characteristic length and $N(L_c)$ is the number of fragments of size equal or larger than L_c. The parameter M_E is here estimated considering that for the two breakups the number of fragments added to the debris population catalog is known (respectively 6 objects for Cosmos 1867 and 4 objects for Cosmos 2428). Therefore, assuming that the tracked fragments are larger than 10 cm, the value of M_E is obtained.

Table 2: Parameters of two recent small breakups [21]

Spacecraft	h_p [km]	h_a [km]	i_0 [deg]	M_E
COSMOS 1867	775	800	65	1.2327
COSMOS 2428	845	860	71	0.71793

For the first breakup, the impact on the target list is shown in Fig. 3, which shows the cumulative collision probability collision probability caused by fragments larger than 1 cm from the time of band formation; the data for Fig. 3 were obtained with a total computational time of 3 minutes on a PC with 8 CPUs at 3.40 GHz.

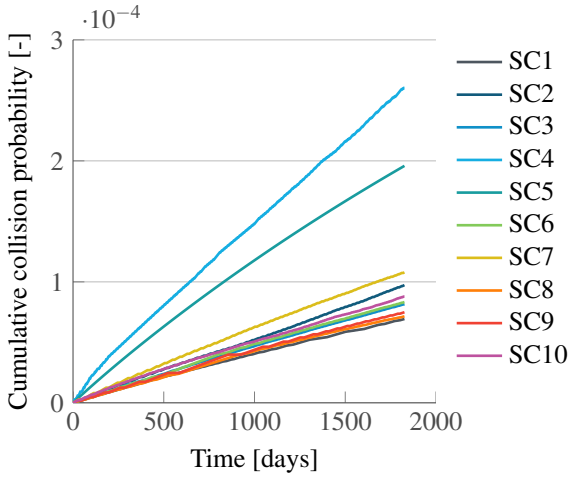

Figure 3: Resulting collision probability from the Cosmos 1867 breakup on the targets in Tab. 1

Fig. 3 suggests that the cross area has a very large influence on the collision probability as the four spacecraft with the largest area (SC4, SC5, SC7, SC2) have also the largest collision probability. The orbits o fthese spacecraft are also quite close to the fragmentation altitude ($\Delta h = 15 - 30$ km), so they cross the fragmentat cloud close to the peak. Interestingly, the spacecraft with the smallest difference in altitude, SC10 ($\Delta h = 6.3$ km) has instead a much lower collision probability than, for example, SC4 (8.8×10^{-5} versus 2.6×10^{-4}). For this spacecraft, in fact, the inclination (85°) is higher than i_0, so it spends part of its trajectory outside the band formed by the debris cloud.

The observation on the effect of the inclination can be drawn also from the simulation of the second breakup, shown in Fig. 4. In Fig. 4a, three spacecraft have the highest cumulative collision probability and they all have semi-major axis and inclination similar to the one of the fragmentation. However, to better highlight the role of inclination, one can compare the behavior of SC5 and SC7, which both have large and similar cross-sectional area. For SC5 the difference in altitude with the fragmen-

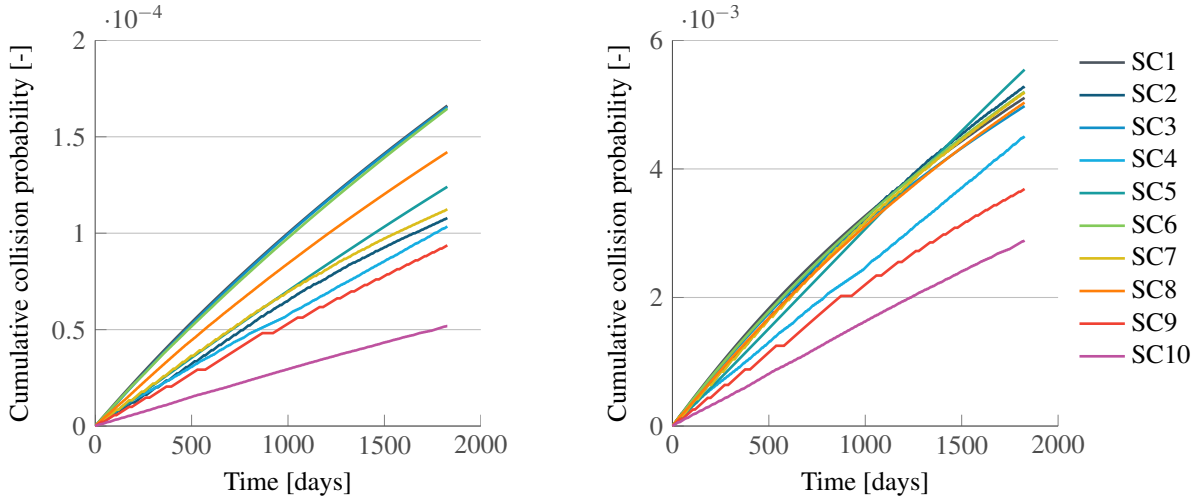

(a) Objects larger than 1 cm

(b) Objects larger than 1 mm

Figure 4: Resulting collision probability from the Cosmos 2428 breakup on the targets in Tab. 1

tation is around 40 km and its inclination is lower than the fragmentation one, so the spacecraft is always inside the fragment band. For this reason, the line of the collision probability appears almost straight, with its slope slowing decreasing because of drag reducing the fragment density. On the other hand, SC7 has higher inclination than the fragmentation, so it is not always inside the fragment band and its curve appears less linear than for SC5. Therefore, even if the difference in altitude is smaller for SC7 ($\Delta h = 25\,\text{km}$) than for SC5, also the collision probability is lower. This suggest that even if it is clear which parameters have an impact on the collision probability, the proposed method can be useful in quantifying their relative importance. In fact, the simple computation of the difference in the orbital parameters between the fragmentation location and the targets' orbits may not always be conclusive to rank the relative risk.

Fig. 4 shows also the comparison between the resulting collision probability from objects larger than 1 cm (Fig. 4a) and larger than 1 mm (Fig. 4b); the results for the latter case were obtained with a computational time equal to 40 minutes on a PC with 8 CPUs at 3.40 GHz.

As expected, the collision probability is much higher if also the smallest fragments are included. In particular, the cumulative collision probability is 33 times higher in the case where all the fragments larger than 1 mm are considered. One cal also observe that now the spacecraft with the largest collision probability is SC5. This result may be explained by the fact theat inclidung all the fragments down to 1 mm, the percentage of fragments with high area-to-mass ration is larger. These fragments decay quicker and so the cloud has a larger impact on spacecraft at low altitudes such as SC5. This observation seem confirmed also by the steep slope in the curve for SC4, which is also on low orbit. In attidion, SC5, differently form SC4, is always inside the fragment band, so it always accumulates collision probability.

4.2. Maps of collision probability

The collision risk for a spacecraft can be studied also from a different point of view: instead of focusing on a single breakup, here the location of the breakup is changed to highlight the impact of the breakup conditions on the collision probability. In particular, here the altitude and the inclination of the fragmentation are changed and this allows defining the most dangerous regions for a collision to occur for all the targets in Tab. 1. Other parameters (e.g., time, fragmentation energy) may be considered with the same approach.

Fig. 5 shows, for example, the study done for the spacecraft SC2 for fragmentations of 100 kJ, including all the fragments down to 1 mm. The peak in the collision probability is at the altitude of the spacecraft semi-major axis ($a_{SC2} = R_E + 817\,\text{km}$) and for the inclination equal and higher than the spacecraft inclination as in this condition the spacecraft is always inside the band formed by the fragments. Fragmentations at higher altitudes than a_{SC2} have a large impact than the ones at lower altitudes. In fact, as with time drag tends to reduce the fragments altitude, the fragments initially at altitudes higher than a_{SC2} decay towards the target orbit. It is also possible to observe how fragmentations at high inclination have a larger impact: the cumulative collision probability is very similar for a fragmentation at 90° and 900 km and for one at 60° and 860 km, even if the latter is 40 km closer to the target.

The same analysis was performed for all the targets in Tab. 1 to obtain the map in Fig. 6. Here it is possible to observe a peak around 840 km, which is the altitude

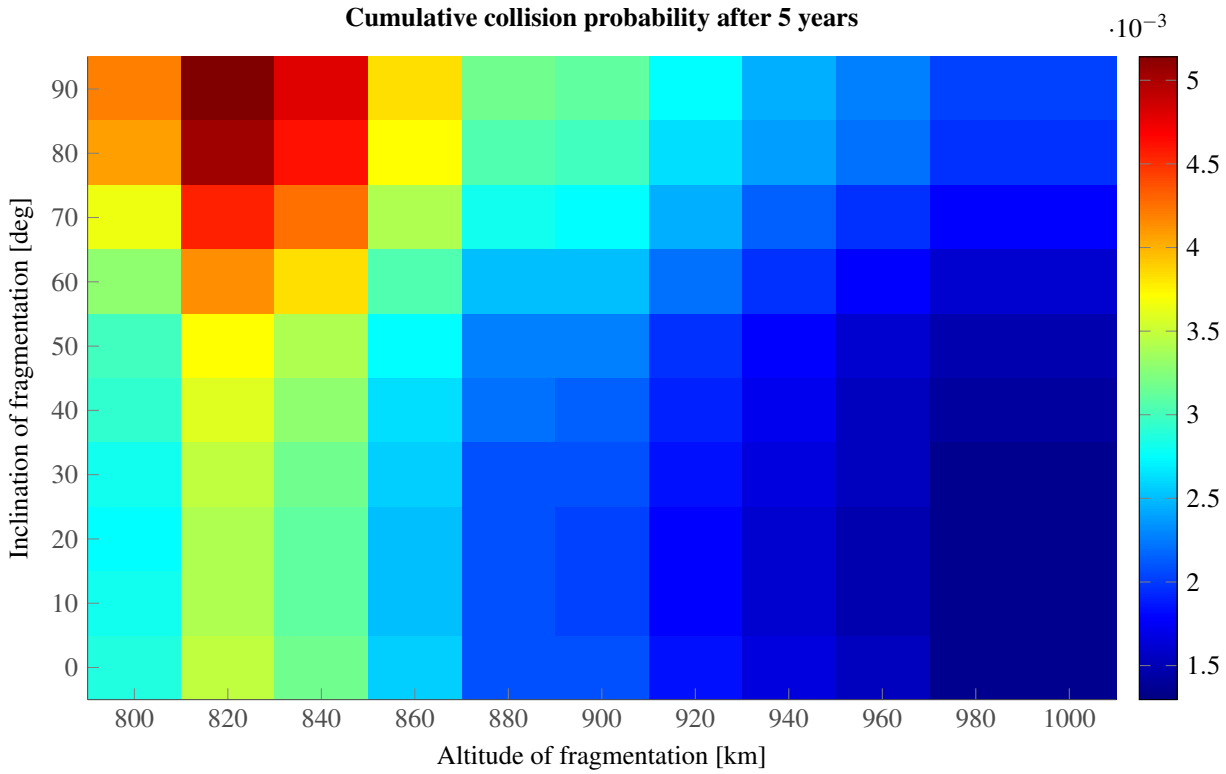

Figure 5: Collision probability map for SC2 for fragmentations of 100 kJ*, including all the fragments down to* 1 mm

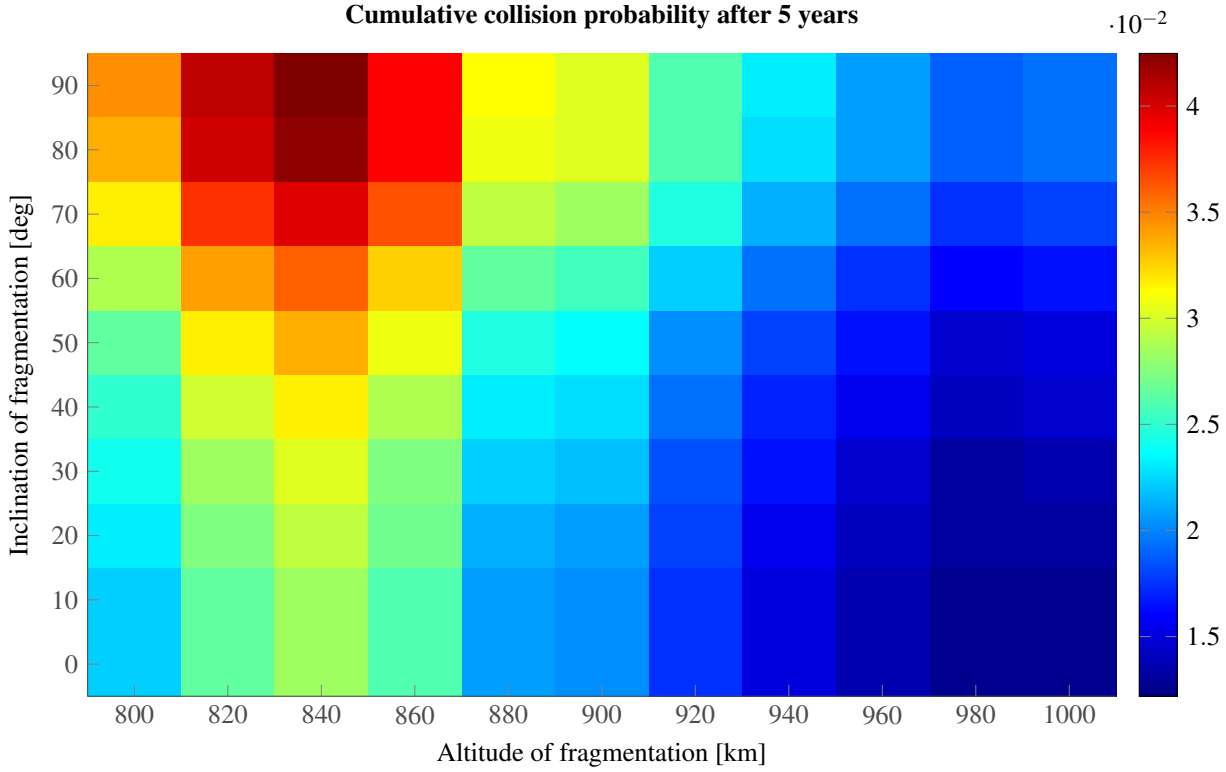

Figure 6: Total collision probability map for the targets in Tab. 1 for fragmentations of 100 kJ*, including all the fragments down to* 1 mm

around where there are four spacecraft in the list (SC1, SC3, SC6, SC8). These spacecraft also have roughly the same inclination (71°), so, as in Fig. 5, the collision probability is maximum for fragmentation occurring at inclinations equal or higher than this value.

The collision probability is high also in the altitude band around 820 km where there are three spacecraft from the list (SC2, SC7, SC9). As explained for Fig. 5, the decay of fragment altitude due to drag increases the impact of fragmentation at high altitudes: the collision probability around 860 km has the same value of the one at 820 km even if there is only one spacecraft close to 860 km and three around 820 km.

A map such as the one in Fig. 5 is obtained with a computational time of around two hours on a PC with 8 CPUs at 3.40 GHz. The process can be easily automatized and parallelized to study a list of targets and obtain a global map as the one in Fig. 6. These maps may be useful to study both operational and non-operational targets to understand under which conditions a fragmentation has the largest impact on the spacecraft. Moreover, the global maps can highlight the most critical areas in terms of influence on the whole spacecraft population and can be used, for example, to identify interesting candidates for active debris removal.

5. CONCLUSIONS

Small debris fragments can pose a relevant hazard in case of collision: fragments larger than 1 mm can cause anomalies to operational spacecraft and impacts with objects larger than 1 cm can even destroy a satellite. However, the number of small fragments in the debris population is too high to follow each single fragment trajectory and so their contribution to the collision probability is often not considered. Moreover, even in a single fragmentation the number of small fragments can be high enough that alternative methods of propagation are more convenient. In this work, a novel approach based on the description of the fragment density was introduced. Changing the point of view from the single fragments to the global evolution of the cloud density allows an important reduction of the computational time thus enabling new analysis on the contribution of small fragments to the collision probability. More in detail, the method was used to evaluate the change in the collision probability of some reference spacecraft due to a fragmentation. The fragmentation, a non-catastrophic collision, was described with the NASA breakup model: the generated fragments are numerically propagated in the beginning until they form a band around the Earth; afterwards, their spatial density is used as state variable of the study and its evolution under the effect of drag only can be obtained analytically. The fragment density is then used to compute the collision probability for a spacecraft crossing the cloud. The method was applied to study the impact of two real breakups on a list of targets, highlighting the dominant influence of inclination. Another application is the simulation of many collision scenarios with different fragmentation conditions, in this case the altitude and the inclination of the orbit where the fragmentations occurred. In this way, a *map* of the collision probability as a function of the fragmentation altitude and inclination can be built for each target and then also for the whole set. These maps can be useful to identify which regions of space have the largest influence on the global collision probability and may suggest interesting targets for active debris removal.

ACKNOWLEDGEMENT

Francesca Letizia would like to thank the Space Generation Advisory Council for the sponsorship that enabled her to participate in the IAASS Conference 2014. Camilla Colombo acknowledges the support received by the Marie Curie grant 302270 (SpaceDebECM - Space Debris Evolution, Collision risk, and Mitigation), within the 7th European Community Framework Programme. The authors acknowledge the use of the IRIDIS High Performance Computing Facility, and associated support services at the University of Southampton, in the completion of this work.

REFERENCES

[1] P. H. Krisko. The predicted growth of the low-Earth orbit space debris environment an assessment of future risk for spacecraft. *Proceedings of the Institution of Mechanical Engineers, Part G: Journal of Aerospace Engineering*, 221(6):975–985, January 2007. doi: 10.1243/09544100JAERO192.

[2] C. Martin, R. Walker, and H. Klinkrad. The sensitivity of the ESA DELTA model. *Advances in Space Research*, 34(5):969–974, January 2004. doi: 10.1016/j.asr.2003.02.028.

[3] A. E. White and H. G. Lewis. The many futures of active debris removal. *Acta Astronautica*, 95: 189–197, February 2014. doi: 10.1016/j.actaastro.2013.11.009.

[4] A. Rossi, A. Cordelli, and C. Pardini. Modelling the space debris evolution: Two new computer codes. *Advances in the Astronautical Sciences-Space Flight Mechanics*, pages 1–15, April 1995.

[5] C. R. McInnes. An analytical model for the catastrophic production of orbital debris. *ESA Journal*, 17(4):293–305, 1993.

[6] N. Gor'kavyi. A new approach to dynamical evolution of interplanetary dust. *The Astrophysical Journal*, 474(1):496–502, 1997. doi: 10.1086/303440.

[7] N. Gor'kavyi, L. Ozernoy, J. Mather, and T. Taidakova. Quasi-stationary states of dust flows under Poynting-Robertson drag: New analytical and numerical solutions. *The Astrophysical Journal*, 488(1):268–276, 1997. doi: 10.1086/304702.

[8] C. Colombo and C. R. Mcinnes. Orbital Dynamics of "Smart-Dust" Devices with Solar Radiation Pressure and Drag. *Journal of Guidance, Control, and Dynamics*, 34(6):1613–1631, May 2011. doi: 10.2514/1.52140.

[9] D. S. McKnight. A phased approach to collision hazard analysis. *Advances in Space Research*, 10(3-4):385–388, January 1990. doi: 10.1016/0273-1177(90)90374-9.

[10] R. Jehn. Dispersion of debris clouds from In-orbit fragmentation events. *ESA Journal*, 15(1):63–77, 1991.

[11] F. Letizia, C. Colombo, and H. G. Lewis. Analytical model for the propagation of small debris objects clouds after fragmentations. *Journal of Guidance, Control, and Dynamics*, 2014. [Accepted].

[12] N. L. Johnson and P. H. Krisko. NASA's new breakup model of EVOLVE 4.0. *Advances in Space Research*, 28(9):1377–1384, 2001. doi: 10.1016/S0273-1177(01)00423-9.

[13] P. H. Krisko. Proper Implementation of the 1998 NASA Breakup Model. *Orbital Debris Quarterly News*, 15(4):1–10, 2011.

[14] C. Colombo and C. R. McInnes. Orbital Dynamics of "Smart-Dust" Devices with Solar Radiation Pressure and Drag. *Journal of Guidance, Control, and Dynamics*, 34(6):1613–1631, May 2011. doi: 10.2514/1.52140.

[15] J. Ashenberg. Formulas for the phase characteristics in the problem of low-Earth-orbital debris. *Journal of Spacecraft and Rockets*, 31(6):1044–1049, November 1994. doi: 10.2514/3.26556.

[16] D. J. Kessler. Derivation of the collision probability between orbiting objects: the lifetimes of Jupiter's outer moons. *Icarus*, 48(1):39–48, October 1981. doi: 10.1016/0019-1035(81)90151-2.

[17] F. Letizia, C. Colombo, and H. G. Lewis. Continuity equation approach for the analysis of the collision risk due space debris clouds generated by a fragmentation event. In *International Astronautical Congress*, Toronto, September 2014. IAC-14.A6.P.31.

[18] D. A. Vallado. *Fundamentals of astrodynamics and applications*. Springer, 4th edition, 2013. Pages 551–573, 619–688. ISBN: 978-1881883180.

[19] S.-Y. Su and D. Kessler. Contribution of explosion and future collision fragments to the orbital debris environment. *Advances in Space Research*, 5(2):25–34, January 1985. doi: 10.1016/0273-1177(85)90384-9.

[20] A. Rossi, G. B. Valsecchi, L. Anselmo, C. Pardini, H. G. Lewis, and C. Colombo. Fragmentation consequence analysis for leo and geo orbits. In *GreenOps Workshop*, Noordwijk, November 2013. ESA AO 1/7121/12/F/MOS.

[21] NASA Orbital Debris Program Office. Flurry of Small Breakups in First Half of 2014. *Orbital Debris Quaterly News*, 18(3):1–2, 2014.